# Nanoparticles as Nonfluorescent Analogues of Fluorophores for Optical Nanoscopy

**Simon Hennig,[†,∥] Viola Mönkemöller,[†,∥] Carolin Böger,[‡] Marcel Müller,[†] and Thomas Huser*[,†,§]**

[†]Biomolecular Photonics, Department of Physics, University of Bielefeld, Universitätsstr. 25, 33615 Bielefeld, Germany, [‡]Institute of Physical and Theoretical Chemistry, Johann Wolfgang Goethe-University Frankfurt, Max-von-Laue-Str. 7, 60438 Frankfurt, Germany, and [§]Department of Internal Medicine, NSF Center for Biophotonics, University of California, Davis, 2700 Stockton Boulevard, Suite 1400, Sacramento, California 95817, United States. [∥]S.H. and V.M. contributed equally to this work.

**ABSTRACT** Optical microscopy modalities that achieve spatial resolution beyond the resolution limit have opened up new opportunities in the biomedical sciences to reveal the structure and kinetics of biological processes on the nanoscale. These methods are, however, mostly restricted to fluorescence as contrast mechanism, which limits the ultimate spatial resolution and observation time that can be achieved by photobleaching of the fluorescent probes. Here, we demonstrate that Raman scattering provides a valuable contrast mechanism for optical nanoscopy in the form of super-resolution structured illumination microscopy. We find that nanotags, *i.e.*, gold and silver nanoparticles that are capable of surface-enhanced Raman scattering (SERS), can be imaged with a spatial resolution beyond the diffraction limit in four dimensions alongside and with similar excitation power as fluorescent probes. The highly polarized nature of super-resolution structured illumination microscopy renders these nanotags elliptical in the reconstructed super-resolved images, which enables us to determine their orientation within the sample. The robustness of nanotags against photobleaching allows us to image these particles for unlimited periods of time. We demonstrate this by imaging isolated nanotags in a dense layer of fluorophores, as well as on the surface of and after internalization by osteosarcoma cells, always in the presence of fluorescent probes. Our results show that SERS nanotags have the potential to become highly multiplexed and chemically sensitive optical probes for optical nanoscopy that can replace fluorophores in applications where fluorescence photobleaching is prohibitive for following the evolution of biological processes for extended times.

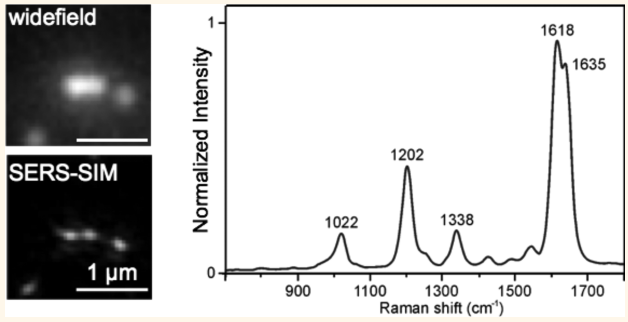


**KEYWORDS:** structured illumination light microscopy · super-resolution optical imaging · surface enhanced Raman microscopy · Raman spectroscopy

To date, fluorescence microscopy is the most widely used molecularly specific imaging technique in the biomedical sciences. This is explained by the relatively low cost of this microscopy modality, its capability for imaging live and fixed samples with a multitude of additional contrast mechanisms and colors, and the wide availability of fluorescent probes. Organic fluorophores are available either as intrinsically specific cellular stains or they can be reacted with a wide selection of biomolecules to render them molecularly specific. Fluorescent proteins can be fused with proteins of interest to result in intrinsically fluorescent samples. Efforts to improve the spatial resolution of this technique have recently been rewarded with the 2014 Nobel Prize in Chemistry. While early implementations of optical nanoscopy, such as stimulated emission depletion (STED) microscopy,[1−3] single-molecule localization microscopy (PALM, (*d*)STORM),[4−6] and (nonlinear) structured illumination microscopy (SIM)[7−10] are already available in a number of commercial systems, other methods, such as fluctuation-based microscopy,[11] and combinations of the original implementations are still being developed. A severe drawback of all fluorescence-based microscopy techniques is, however, the rapid photobleaching of organic fluorophores. Solutions to minimize this problem, *i.e.*, oxygen-scavenging systems, can be utilized, but

* Address correspondence to thomas.huser@physik.uni-bielefeld.de.

Received for review March 10, 2015 and accepted May 7, 2015.

**Published online May 07, 2015**
**10.1021/acsnano.5b01503**

the underlying photochemical process cannot be entirely avoided, and, especially in live cell imaging, this still remains a significant problem for super-resolution microscopy. Alternatives to organic fluorophores, such as semiconductor quantum dots (Qdots)[12] or fluorescent nitrogen vacancy (NV) centers in nanodiamond particles,[13,14] have been explored, but Qdots still exhibit some degree of photobleaching (although at reduced rates) and NV nanodiamond particles are fairly large and cannot be multiplexed. Another alternative presents itself in the use of Raman-active nanoparticles.[15] Raman scattering, the inelastic scattering of light by molecular bonds, results in Stokes and anti-Stokes scattered photons, where Stokes scattering is significantly stronger at room temperature. The scattered photons resemble a spectrum with sharp spectral lines that can be attributed to vibrations of different Raman-active groups within the sample. While spontaneous Raman scattering from biological samples by itself is typically too weak to serve as an alternative to fluorescent probes, enhancement mechanisms, such as coherent Raman scattering (CRS)[16,17] or surface-enhanced Raman scattering (SERS)[18] can produce signal strengths close to those observed from fluorescently labeled samples. Specifically, SERS nanotags, *i.e.*, surface plasmon resonant gold or silver nanoparticles coated with an organic molecule that provides the Raman signature, can be targeted against biomolecules and could serve as a photostable, highly multiplexed optical probe.[19−22]

Here, we explored the potential of using SERS tags as alternative labels for structured illumination microscopy. Super-resolution structured illumination microscopy (3D-SIM) uses illumination patterns with a periodicity close to the optical diffraction limit, typically generated as interference patterns, to excite fluorescence or, in our case, Raman scattering in a sample. The signal is collected as wide-field images and contains mixed spatial frequencies of the illumination pattern and the sample. If the down-shifted frequencies of sample structures below the diffraction limit can be identified and isolated, then a new image with up to twice the previous spatial resolution can be reconstructed.[8] This method is attractive because it is very signal-efficient by collecting wide-field images with high numerical aperture microscope objective lenses and using single-photon-counting cameras. Also, it requires a low number of images, between 6 and 15, obtained for each *z*-plane within a sample to reconstruct the higher-resolution image. 3D-SIM has already been implemented in commercial microscopes and has been used to image biological samples, such as the structure of the nuclear envelope,[7] the clustering of DNA-repair enzymes within bacterial cells,[23] fenestrations in liver sinusoidal endothelial cells in fixed cells,[24,25] or the movement of the cytoskeleton and mitochondria in living cells,[26−28] to name just a few. To overcome limitations imposed by photobleaching in all of these applications, we imaged SERS nanotags with 3D-SIM and compared their signal strength and signal persistence against those of commonly available fluorescent stains optimized for improved photostability. We find that SERS nanotags can indeed be used as photostable analogues to fluorescent dyes for super-resolution microscopy of biological samples and offer additional benefits, such as the higher potential for multiplexing due to their spectrally narrow signatures[20] and chemical sensing capabilities.[29,30]

## RESULTS

**3D Structured Illumination Microscopy of SERS Nanotags on a Glass Substrate.** The potential of SERS nanotags to provide sufficient signal and contrast for super-resolution imaging by three-dimensional structured illumination microscopy (3D-SIM) was first investigated by depositing SERS nanotags onto a glass coverslip surface. The SERS nanotags are composed of 50 nm gold particles coated with *trans*-1,2-bis(4-pyridyl)ethylene (BPE) and surrounded by a $SiO_2$ shell.[19] The SERS nanotags were deposited onto the coverslip surface by allowing 10 $\mu$L of a 1:10 dilution of SERS nanotags in water to evaporate for 30 min at room temperature. This results in a glass surface with varying nanotag coverage: dense near the border of the droplet and less dense near the center of the droplet. For our initial imaging experiments, we chose an area with a nanotag coverage of approximately 0.1 particles/$\mu m^2$ (Figure 1a,b). Images of the SERS nanotags were taken on a commercial 3D-SIM setup (DeltaVision|OMX V4-BLAZE, GE Healthcare, Amersham, UK). The wide-field images were obtained using standard wide-field illumination power density (approximately 20 W/$cm^2$) by exciting the SERS nanotags at 642 nm. Upon excitation at 642 nm, the SERS nanotags emit their characteristic SERS spectrum, as shown in Figure 1d. The Stokes-shifted SERS signal of the SERS particles was collected using a 683/40 bandpass filter and imaged by a sCMOS camera. Individual SERS nanotags are clearly visible as white spots in the wide-field image (Figure 1a) and the 3D-SIM reconstruction (Figure 1b). However, as the insets to both images show, particles that are in close proximity (below the optical diffraction limit) cannot be resolved by wide-field microscopy, whereas the 3D-SIM reconstruction clearly identifies the particles as individual SERS nanotags. This is further confirmed by the comparison of the respective cross-sections through the particles, shown in Figure 1c. The distance between the particles is approximately 280 nm, as measured by 3D-SIM, which clearly is not sufficient to fully separate the particles in the wide-field image.

Interestingly, as becomes particularly evident from the enlarged view in the inset of Figure 1b, the SERS nanotags are reconstructed with an elliptical shape in the 3D-SIM image, whereas the wide-field image shows the particles as round spots. This behavior

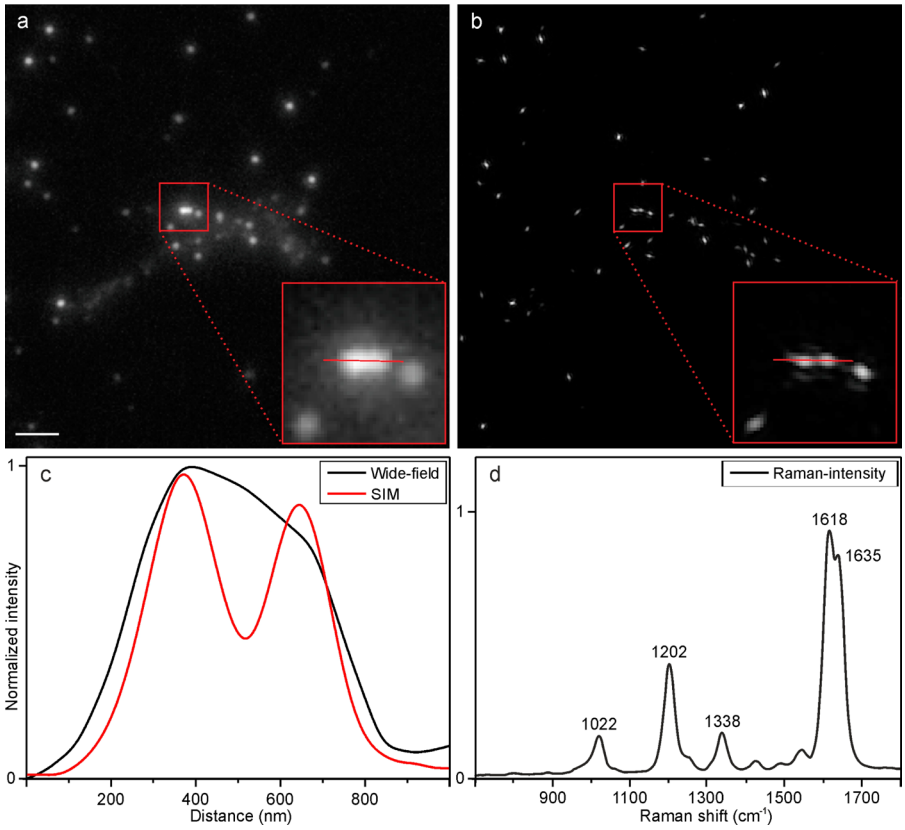


**Figure 1. SERS nanotags imaged by 3D structured illumination microscopy (3D-SIM) after depositing on a glass coverslip surface and mounting in glycerol. Images were acquired by exciting SERS nanotags at 642 nm and detecting the Stokes-shifted Raman signal through a 683/40 nm bandpass filter using a 1.49 NA microscope objective lens. (a) *Z*-projection of a conventional wide-field image of the SERS tags. The projected image consists of eight single planes. (b) 3D-SIM reconstruction of the same area shown in (a). Single SERS nanotag particles can be clearly distinguished in the high-resolution image (see inset). (c) Cross-sections of the two particles shown in the insets of (a) and (b). Only the SIM reconstruction is able to separate the particles. (d) Surface-enhanced Raman spectrum of the nanotags. The particles show the typical SERS fingerprint spectrum of *trans*-1,2-bis(4-pyridyl)ethylene with well-separated vibrational peaks, as indicated by their Raman-active modes in the figure. Scale bar: 2 $\mu$m.**

becomes even more apparent when we directly compare the spot dimensions of a single SERS nanotag in the wide-field and 3D-SIM images (Figure 2). Here, the 3D-SIM reconstruction appears highly excentric with a long axis along the vertical direction running from the lower left to the upper right of the image. A comparison of the cross-sections indicated in Figure 2a,b shows both the higher spatial resolution achieved by 3D-SIM as well as the elliptical artifact. Figure 2c compares the short axes of the images. The full width at half-maximum (fwhm) of the particle in the wide-field image measures approximately 254 nm (purple line), whereas the fwhm of the particle along the same axis in the 3D-SIM reconstruction measures 107 nm, resulting in a difference in apparent spatial resolution by a factor of approximately 2 in this direction. In the direction perpendicular to this, the particle diameter (fwhm) in the wide-field image measures 268 nm (green line), whereas the 3D-SIM reconstruction results in a width of 182 nm (blue line), resulting in only a 1.5× difference in spatial resolution. Figure 2e shows the discrepancy between the particle diameters measured by 3D-SIM by directly comparing the two cross-sections. Here, the difference in the reproduction of the width of the particle leads to an excentricity of 0.26.

As will be explained and verified in the following, we attribute this behavior to a reconstruction artifact due to the highly sensitive response of the SERS signal intensity to the polarization of the excitation light. As is well-known by now and as has been shown by multiple authors, SERS nanoparticles exhibit their maximum enhanced SERS signal intensity when the organic molecules giving rise to the Raman spectrum are located in the junction between two gold (or silver) nanoparticles.[31,32] These nanoparticles thus form a nanoparticle dimer, and the maximum enhancement of the electromagnetic field is achieved if the surface plasmons within the metal particles are excited along the dimer axis, *i.e.*, if the polarization is parallel to the dimer axis.[19] For an excitation polarization perpendicular to the dimer axis, the SERS signal intensity will be minimal. The algorithm used to reconstruct 3D-SIM data, however, expects equal signal intensities for all angles of the SIM illumination pattern.[8] Low signal-to-noise ratios result in a reconstruction with a poorer spatial resolution in the 3D-SIM image. In 3D-SIM, however, in order to

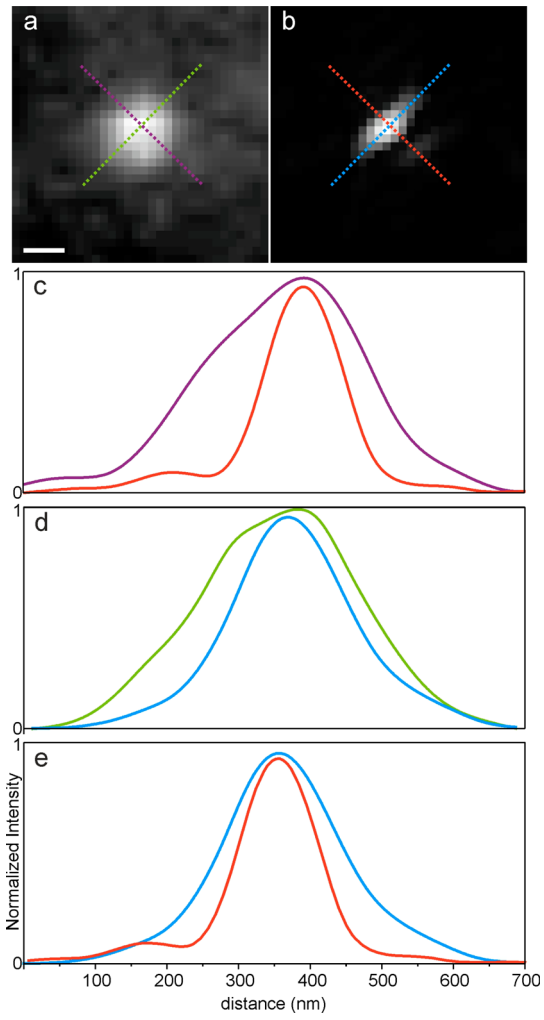


**Figure 2. Comparison between the (a) wide-field image and (b) 3D-SIM reconstructed image of a single SERS nanotag. The colored dashed lines in the images indicate the directions of the cross-sections shown in the plots below. (c) Comparison between the cross-section along the wide-field (purple) and 3D-SIM (red) images running from the upper left to lower right corner. (d) Comparison between the cross-section along the wide-field (green) and 3D-SIM (blue) images running from the upper right to lower left corner. While the particle in the wide-field image appears to be fairly round with full width at half-maxima (fwhm) of 254 and 268 nm along the purple and green cross-sections, the fwhm of the SIM reconstruction are 107 nm (red) and 182 nm (blue). (e) Cross-sections of the SIM reconstruction shown for comparison. The graph clearly shows the difference in optical resolution along different directions within the SIM image. Scale bar: 200 nm.**

achieve the best contrast ratios for the interference patterns used as excitation patterns, the beams are linearly polarized. This polarization is rotated along the angles of illumination for each of the three angles used to obtain the 3D-SIM raw images. For the axis exactly perpendicular to the direction of the vector describing the orientation of the interference pattern, the SERS signal will be maximum. If, however, the SERS nanotag is oriented with its dimer axis parallel to the vector describing the interference pattern, then the SERS signal intensity will be minimal. This results in a highly elliptical reconstruction of the particle with a short axis (high spatial resolution) achieved for the high signal contrast and a poor spatial resolution obtained for the perpendicular direction. We have verified this behavior by assigning different colors (red, green and blue) to the images obtained for the three different excitation angles used for 3D-SIM and by overlaying these colors with the 3D-SIM reconstruction of the particle images. The result is shown in Figure 3, where the colored arrows indicate the polarization for the different angles. Here, the SERS nanotags appear as a blend of the different colors assigned to the angles. As shown in the enlarged view in Figure 3b, the long particle axes clearly correspond to the different excitation angles, which verifies the highly polarization-dependent 3D-SIM reconstruction of SERS nanotags.

Despite this artifact, SERS nanotags still produce signal intensities rivaling those of organic fluorophores, yet they exhibit no photobleaching. This is shown in Figure 4, where U2OS cells were fixed and subsequently stained with Alexa 488—phalloidin. After applying the fluorescent stain and three washing steps with PBS, SERS nanotags were applied to the sample and allowed to settle on the cell's surface. Using 3D-SIM, we were able to record structured illumination images from both sources, Alexa 488 and SERS particles, and compare their signal strengths against each other. Images are collected by exciting Alexa 488 with 0.1 kW/cm$^2$ for 10 ms and the SERS nanotags with 3 kW/cm$^2$ for 400 ms. Successful reconstruction of both channels using the set of SIM raw data obtained at the start of the experiment is shown in Figure 4a. Here, the Alexa 488 stain exhibited its brightest signal. Figure 4b shows the same field of view using the same stains, after illuminating both stains for 30s with approximately 1 kW/cm$^2$ laser power in the blue and approximately 3 kW/cm$^2$ laser power in the red excitation channels. As can be seen by the dramatic difference in contrast in Figure 4b, the Alexa 488 channel, although excited at even lower power than the nanotags, exhibited significant photobleaching after just 30 s, leading to a greatly reduced fluorescence signal. In contrast, the SERS signal remained at the same intensity level throughout the experiment, resulting in reliable reconstructions of the nanotags against the cell's background. This clearly demonstrates the potential of SERS nanotags as photostable analogues of fluorophores.

**Photostability of SERS Nanotags.** The use of conventional organic fluorophores and fluorescent proteins is plagued by rapid and irreversible photobleaching of the fluorescence. Typically, this is caused by a photoinduced reaction of the fluorophore in the excited state with molecular oxygen and can be reduced by using oxygen-scavenging systems (*e.g.*, glucose oxidase/glucose catalase) in the imaging buffer.[33] Especially in the case of live cell imaging experiments, however,

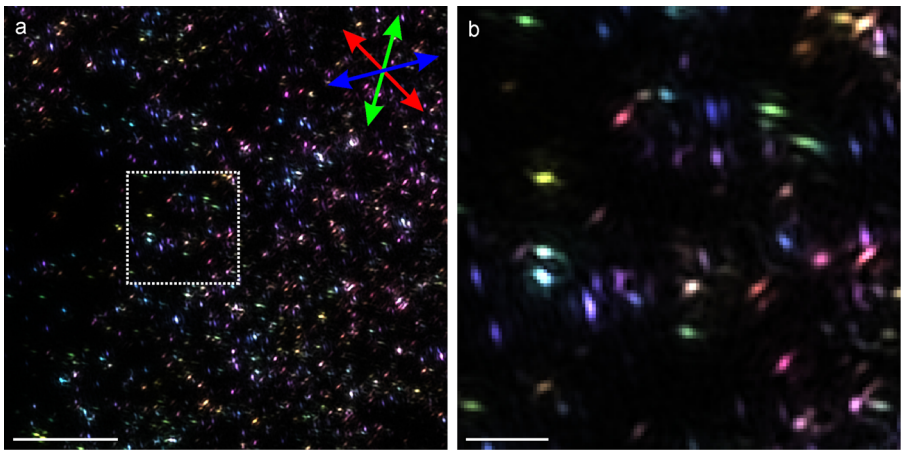


**Figure 3. Color-coded 3D-SIM reconstructions of SERS nanotags on a glass substrate. Red, green, and blue indicate the different angles (and therefore linear polarizations) at which the SIM data were acquired. (a) 3D-SIM overview of the SERS particles. Scale bar: 5 $\mu$m. (b) Zoomed view of the area highlighted in (a) by a white-dashed frame. Scale bar: 1 $\mu$m.**

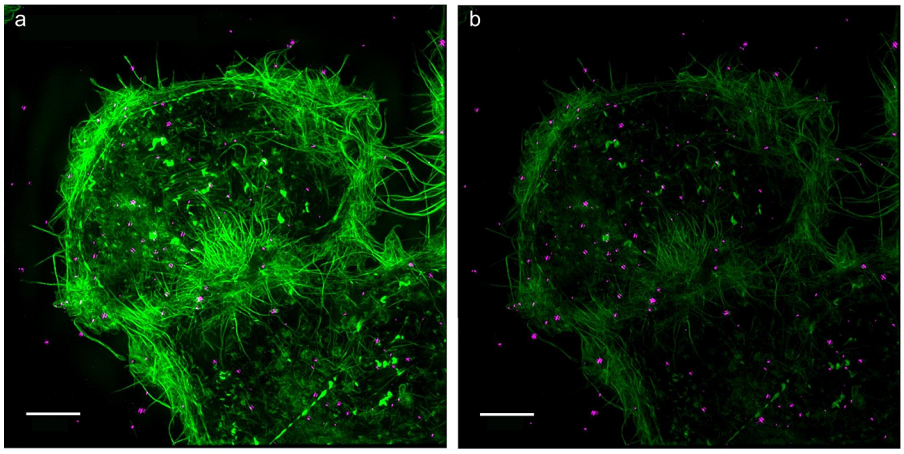


**Figure 4. Two-color *z*-projection of a 3D-SIM image of SERS nanotags (shown as magenta dots) lining a U2OS cell, where the actin cytoskeleton was stained with Alexa Fluor 488—phalloidin (green). (a) The signal strength of the SERS nanotags in 3D-SIM mode is comparable to that of the fluorescent stain, making the SERS tags easily distinguishable even against heavily stained samples. (b) SIM image of the same cell after 30 s of continuous illumination with approximately 1 kW/cm$^2$ laser power density at 488 nm and approximately 3 kW/cm$^2$ laser power density at 642 nm, acquired using the same conditions as in (a). The difference in brightness clearly shows the stability of the SERS nanotags against photobleaching in contrast to the Alexa 488 fluorophore. Scale bars: 5 $\mu$m.**

the use of oxygen scavengers is also detrimental to cell health. Photobleaching is a particular problem for super-resolution microscopies because pretty much all modalities require either the acquisition of multiple images or utilize rather high laser powers. Even 3D-SIM, which typically requires the lowest number of raw images to achieve a modest improvement in spatial resolution, suffers from this problem, leading to artifacts in the reconstruction of super-resolved images.[34] In order to establish the long-term photostability of SERS nanotags, we evaluated them by continuously taking wide-field images of a glass surface coated with a mixture of AlexaFluor 647 and SERS nanotags. Alexa 647 was chosen because, in this case, both the fluorophore and the nanotags can be excited by the same laser excitation wavelength, enabling the direct comparison of their long-term signal stability. For these measurements, the mixture of SERS nanotags and Alexa 647 dyes on a coverslip was illuminated with a power density of 1 kW/cm$^2$ at 643 nm. The fluorescence and SERS signals were detected simultaneously with a single EMCCD camera. At the beginning of the measurement, signals from both types of particles are approximately equal in intensity (Figure 5). Within about 10 s following the start of the continuous exposure, a decrease of the fluorescence signal is noticeable, and four bright spots identifying the location of the SERS nanotags become visible. Within 50 s of continuous illumination, most of the fluorescence has vanished. From this point on, only some faint blinking of the Alexa dyes can be detected. After ~160 s, however, the intensity of the SERS nanotags reaches a stable value of ~60% of their initial brightness and remains stable at this level until the end of the measurement. As shown in the Supporting Information (Figure S1 and accompanying text), the SERS signal of

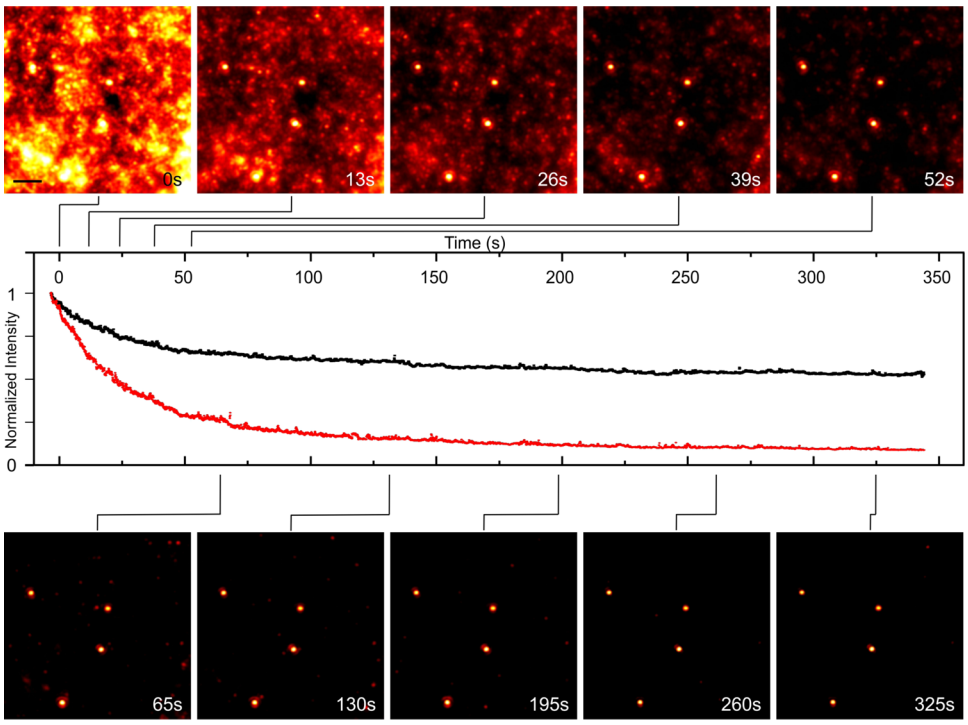


**Figure 5. Time-lapse image sequence of a mixture of SERS nanotags and organic fluorophores deposited onto a dry glass surface. SERS nanotags and Alexa Fluor 647 were dried on a cover glass surface and excited with ~1 kW/cm$^2$ at 643 nm. Both signals were detected simultaneously in the same channel at a frame rate of 15 Hz. Tracking the fluorescence and Raman intensity with time clearly shows the stability of SERS particles (four separated spots) in contrast to that of conventional fluorescent dyes. At the beginning of the measurement, the normalized signals taken at the location of a SERS nanoparticle (black curve) and a location of purely fluorescent dye (red curve) both start at a relative intensity of 1. After about 25 s (500 frames), the fluorescence intensity has decreased to 50% of its initial value. After ~50 s, the fluorescence has almost fully vanished. Altogether, the fluorescence intensity decreases to ~5% of its initial value. In contrast, the Raman signal is still well-detectable after 350 s. It stabilizes at 60% of its initial value after approximately 160 s, representing the remaining SERS signal after the surrounding fluorescence contributions are photobleached. Graphical data were obtained by selection of a representative area for the fluorescence plot and selection of small areas containing the four individual spots with the SERS nanotags. Scale bar: 2 $\mu$m.**

the nanotags can decrease depending on the illumination power. For high illumination powers (0.5 and 2.6 kW/cm$^2$; Figure S1a,d), an initial decrease in the SERS nanotag signal intensity was found. For lower illumination intensities (0.1 and 0.02 kW/cm$^2$), the SERS intensity levels remain stable. Expansions into the timetrace of the SERS signal show no blinking or major fluctuations down to a time scale of 3 ms (Figure S1a, i–iii).

We explain this behavior by first noting that the Raman-active probe molecule used for these nanotags, BPE, has an electronic absorption maximum at approximately 300 nm and no measurable absorption above 350 nm.[35] Thus, this molecule is entirely nonresonant for illumination at 642 nm and cannot photobleach at this wavelength. There are, however, other mechanisms leading to a reduction in intensity of the SERS signal, such as photoinduced molecular motion of the molecule due to repeated trans–cis or cis–trans isomerization.[36] This process does, however, also require resonant excitation of the molecule, which is not the case here. Another possibility is detachment of the molecules from the nanoparticle surface due to photoactivation of the molecule (unlikely for nonresonant excitation) or absorption-induced heating of the nanoparticles based on their plasmon-induced absorption. The primary plasmon resonance of 50 nm gold nanoparticles exhibits a peak at 530 nm, whereas the peak of the quadrupole plasmon resonance in the case of dimerized gold nanoparticles depends on the distance between the nanoparticles and the electric permittivity of the environment.[32] For dimer-like nanoparticles in aqueous solution separated by BPE, the plasmon resonance peaks at 680 nm or higher wavelengths.[19] In our setup, the imaging wavelength of 642 nm excites the nanotags on the leading edge of the quadrupole resonance. Exciting the particles closer to the peak resonance should boost the SERS signal even further, but this is currently not possible with our system. The power dependence of our SERS signal stability measurements shown in the Supporting Information (Figure S1) does, however, suggest that there is a limit to the maximum power with which nanotags can be excited, likely due to thermal degradation of the particles themselves as well as the adsorbed molecules.

**3D Structured Illumination Microscopy of SERS Nanotags Internalized by Cells.** To demonstrate that SERS nanotags can also be used after internalization in cell imaging

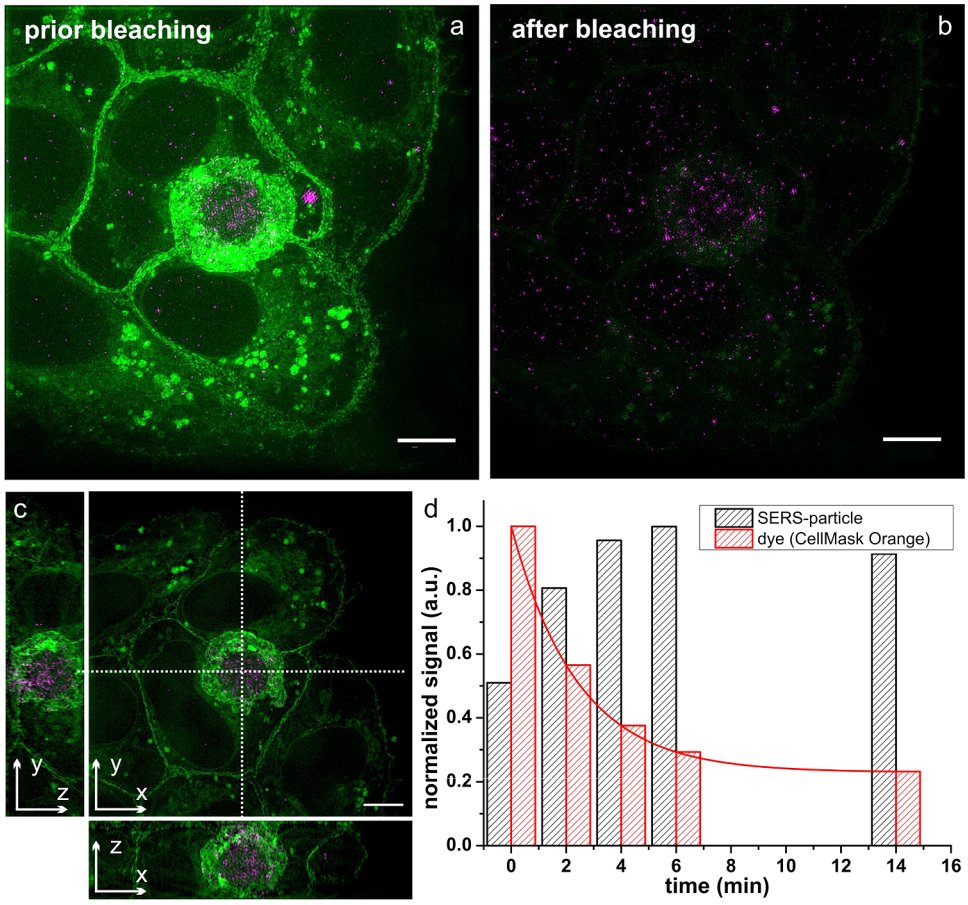


**Figure 6. 3D-SIM fluorescence and SERS images of living U2OS cells incubated with SERS nanotags for 24 h. (a) 3D-SIM reconstruction of the U2OS cells (stained with CellMask Orange, shown in green) and SERS nanotags internalized by the cells (magenta) (b) 3D-SIM reconstruction of the same cells after 14 min of continuous illumination. (c) 3D view as image cross-sections along the *xy*, *xz*, and *yz* directions of same U2OS cells. As can be seen by the *xz* and *yz* views, all SERS nanotags have been internalized by the cells. Dashed lines in the *xy* image indicate the position of the cross-sections. (d) Normalized intensity plot of the different channels following a 14 min illumination sequence. Whereas the fluorescent stain exhibits exponential photobleaching, the SERS nanotags are robust against photobleaching. Scale bars: 5 $\mu$m.**

applications, we conducted an initial proof-of-concept experiment. Here, U2OS cells, an osteosarcoma cell line, were incubated with SERS nanotags for 24 h to allow the cells to take up and internalize the nanotags. Prior to imaging, the cells were fixed with 4% PFA and the membrane of the U2OS cells was stained with CellMask Orange (Life Technologies, Carlsbad, CA, USA). Each stain was imaged in its own color channel, *i.e.*, excitation of CellMask Orange at 568 nm and that of the SERS nanotags, at 642 nm. The cells were imaged by 3D-SIM before and after several bleaching steps, within which the fluorescence signal of CellMask Orange decreased dramatically, while the SERS nanotags maintain high brightness. This is demonstrated in Figure 6, where Figure 6a shows an overlay of the CellMask membrane stain (green) with the SERS nanotags (purple). Figure 6b shows an image of the same cells after 14 min total bleaching time. The spectral separation between the stains enabled high-contrast imaging in each channel, respectively, with insignificant crosstalk between channels. The largest concentration of SERS nanotags is found in the cell in the middle of the image. The surrounding cells, however, also contain nanotags, albeit at lower concentration. These particles have truly been internalized by the cells, as can be seen in Figure 6c, where we show cross-sectional views of the cells. SERS nanotags are clearly found in central locations within the cells, as is evident from the *yz* and *xz* cross-sections shown to the left and at the bottom of the *xy* image in Figure 6c. To further assess the signal strengths of the different stains, Figure 6d shows a normalized intensity plot of the different signals, where signal intensities were summed over the field of view in order to compensate for particle diffusion in the 3D-SIM projections. Time point 0 min is the initial *z*-projection of a 3D image (Figure 6a). Then, three bleaching steps of 2 min followed, and after every step, a measurement was conducted (time points: 2, 4, and 6 min). To correlate the temporal behavior of the photobleaching, equal laser powers were used in both channels. The final bleaching step took another 8 min of illumination, and the result was imaged at time point 14 min (Figure 6b). While the intensity of CellMask Orange decreases

rapidly with the typical exponential decline found for high concentrations of organic fluorophores, the intensity of the SERS nanotags remained at a high level and, if anything, appears to have increased during the image sequence. These results show that SERS nanotags provide sufficient signal strength for wide-field imaging even against the background of fluorescent stains and the autofluorescence of cells.

## CONCLUSIONS AND OUTLOOK

In this article, we have demonstrated that SERS nanotags provide excellent and robust signal-to-noise ratios for imaging applications. These probes have, in particular, proven their suitability for super-resolution microscopy applications, where photobleaching of organic fluorophores is of concern and imposes a significant limitation. SERS nanotags, on the other hand, prove to be highly robust against photobleaching when excited outside any electronic resonances of the organic probe molecules that provide their Raman signature. Although we have not yet taken advantage of this property, their narrow spectroscopic signature should allow for multiplexed imaging of several tens of nanotags with different probe signatures simultaneously, if narrow bandpass filters are employed for imaging. Also, by implementing a ratiometric imaging modality, where different Raman peaks of the same nanotag are imaged onto different color channels, these particles could be used as local probes of their local environment.[30] By functionalizing the outer shell of the $SiO_2$-coated nanotags, they can be directed against specific proteins on the surface or within the cytoplasm of cells.[20] If the physical size of the nanotags is of concern, small silver nanoclusters, often termed Ag nanodots,[37−41] providing similar spectrally narrow signatures should also prove to be quite useful as alternative sources for super-resolution optical microscopy. We believe that such probes will pave the way into the future of live cell imaging applications for optical super-resolution microscopy, as they are only now beginning to also become commercially available.

## MATERIALS AND METHODS

**SERS Nanotags.** The SERS nanotags used in this work were synthesized according to procedures established by Mulvaney and colleagues[42] and were provided to us as a gift by BD Biosciences. A solution of the SERS nanotags in doubly distilled water, derived at a dilution of 1:10 from the stock solution, was typically used for our experiments. For the SERS nanotag surfaces (Figures 1−3), 10 $\mu$L of the 1:10 dilution was spread across the surface of a #1.5 coverglass. After evaporation of the liquid, the dry sample was mounted in glycerol on a glass slide and sealed with nail polish. For Figure 5, 10 $\mu$L stock solution of SERS nanotags were diluted with 10 $\mu$L of $10^{-7}$ M Alexa 647 dissolved in $H_2O$. The sample was subsequently dried on a coverslip at room temperature.

**Measurement of SERS Spectra.** Spectra of the SERS nanotags were acquired on a custom-built confocal microscope setup consisting of an Olympus IX71 inverted optical microscope equipped with a 60× UPLSAPO, 1.2 NA water objective (Olympus, Japan). The SERS nanotags were excited using the 647 nm line of an $ArKr^+$ laser running on all modes. The 647 nm line of the laser was selected with an acousto-optic tunable filter (AOTF, AOTFnCVIS-TN, A-A Opto Electronic). A 647/5 nm bandpass filter was used as an excitation filter, and a FF590/659-Di-01 (Chroma Technology Corp., USA) dichroic mirror in combination with a 655 nm long-pass filter was used to separate the laser excitation from the resulting SERS signals. The signal of individual SERS nanotags was analyzed by routing the light into an optical multimode fiber (AFS 105/125Y, ThorLabs, USA) to deliver it to an ACTON SpectraPro 2300i (Princeton Instruments, USA) spectrometer equipped with 600 l/mm grating blazed for maximum reflectivity at 1 $\mu$m wavelength. Spectra were obtained by a cooled EM-CCD camera (Newton, Andor Technologies, Belfast, Northern Ireland) with a pixel resolution of 1024 × 256 pixels and a pixel size of 26 × 26 $\mu m^2$. The camera was cooled to −80 °C during the measurements. Calibration of the spectrometer was achieved by using toluene at room temperature as a standard.

**3D-SIM Imaging.** 3D-SIM measurements of surfaces coated with SERS nanotags were carried out on a commercial 3D-SIM system (DeltaVision|OMX V4-BLAZE, GE Healthcare, Amersham, UK), equipped with 4 sCMOS cameras for detection of four different color channels simultaneously. The 3D-SIM reconstructions are done with the OMX-specific SoftWoRx software package for image processing. SERS nanotags were excited at 642 nm, Alexa 488−phalloidin was excited at 488 nm, and CellMask Orange was excited at 568 nm. The intensities and exposure times were set to obtain satisfactory signal strengths in every channel. A sequence of 15 images for each *z*-slice, obtained at three different angles with five phases each, was required to successfully reconstruct the nanotag images. Typically, the images used in this article are maximum intensity projections of a 1 $\mu$m stack constisting of eight sections of 125 nm thickness.

**Cells.** Human osteosarcoma cells (U2OS) were incubated in Dulbecco's modified Eagle's medium (DMEM) for 24−48 h at 37 °C and 5% $CO_2$ prior to use. For uptake studies, the cells were incubated overnight (24 h) with SERS nanotags by adding 2 $\mu$L of the nanotag solution to 500 $\mu$L of cell culture medium.

**Fluorescent Staining of U2OS Cells.** For the sample in Figure 4, U2OS cells were plated on cover glass (#1.5, high precision, 170 ± 5 $\mu$m) and incubated at 37 °C in a 5% $CO_2$ environment overnight. Before fixing with 4% PFA for 10 min, the cells were washed with prewarmed PBS. After fixation, the cells were washed again with PBS three times. For actin filament staining, the cells were incubated with Alexa 488−phalloidin for 20 min at room temperature. Subsequently, the cells were washed three times with PBS. After this, the PBS was removed, and 1 $\mu$L of the highly concentrated SERS nanotag stock solution was added to the cells. Finally, the sample was mounted in Vectashield, and the cover glass was sealed onto a slide with nail polish.

The cells shown in Figure 5 were seeded in Labtek slides and incubated at 37 °C in a 5% $CO_2$ environment overnight. Subsequently, 2 $\mu$L of the SERS nanotag stock solution was added to 500 $\mu$L of DMEM, which was added to the living cells. After incubation with the SERS particles, the cells were washed with prewarmed PBS and fixed with 4% PFA (at 37 °C, 5% $CO_2$). After removing the PFA and washing several times with PBS, the sample was incubated with CellMask Orange at a 1:10000 dilution for 10 min. After thoroughly washing with PBS, the sample was imaged in PBS.

**Photostability Measurement of SERS Nanotags.** The investigation of the stability of SERS nanotags (Figure S1) was achieved using a home-built wide-field microscopy setup, using the 647 nm laser line of an $ArKr^+$ laser in combination with a 647/5 nm bandpass filter for excitation. The SERS signal was collected

using a 60× 1.49 NA oil immersion objective (Olympus, Japan) and detected by an IXON+ EMCCD camera (Andor Technologies, Ireland), run at −80 °C with use of the Andor Solis software package for image acquisition. For separation of the excitation line and the resulting SERS signals, a FF560/659 dichroic mirror in combination with a 655 nm long-pass and a 700/75 nm bandpass filter was used. The mixture of Alexa dyes and SERS particles on dry glass surfaces in Figure 5 was excited by a diode laser (Toptica, Germany) at 643 nm and detected with the filter set described above.

**Fluorescent Probes.** CellMask Orange, Alexa 488−phalloidin, and Alexa Fluor 647 were purchased from Life Technologies (Carlsbad, CA, USA).

**Data Analysis.** Cross-sections in Figures 1 and 2 were smoothened by using a *b*-spline approximation for distinct representation of the results. To compare wide-field images with SIM images, the wide-field images were expanded to the pixel size of the SIM images.

*Conflict of Interest:* The authors declare no competing financial interest.

*Supporting Information Available:* Figure S1: Photostability of single SERS tags under wide-field illumination conditions. The Supporting Information is available free of charge on the ACS Publications website at DOI: 10.1021/acsnano.5b01503.

*Acknowledgment.* This work was supported in parts by the Ministry of Innovation, Science, Research and Technology of the State of North Rhine-Westphalia (MIWFT) as part of the research cooperation "MoRitS—Model-based Realization of intelligent Systems in Nano- and Biotechnologies" (grant no. 321-8.03.04.03-2012/02). Additional support was provided by grant no. KF2140605AB3 of the German Federal Ministry for Economic Affairs and Energy. The purchase of the DeltaVision|-OMX super-resolution microscope was supported by grant no. INST 215/435-1 FUGG from the German Research Foundation (DFG). We would like to thank Saskia Bannister for the preparation of cells and Dr. Wolfgang Hübner for additional technical support with the OMX and helpful discussions about image reconstruction and image representation.

## REFERENCES AND NOTES

1. Hell, S. W.; Wichmann, J. Breaking the Diffraction Resolution Limit by Stimulated-Emission—Stimulated-Emission-Depletion Fluorescence Microscopy. *Opt. Lett.* **1994**, *19*, 780–782.
2. Klar, T. A.; Jakobs, S.; Dyba, M.; Egner, A.; Hell, S. W. Fluorescence Microscopy with Diffraction Resolution Barrier Broken by Stimulated Emission. *Proc. Natl. Acad. Sci. U.S.A.* **2000**, *97*, 8206–8210.
3. Hell, S. W. Far-Field Optical Nanoscopy. *Science* **2007**, *316*, 1153–1158.
4. Betzig, E.; Patterson, G. H.; Sougrat, R.; Lindwasser, O. W.; Olenych, S.; Bonifacino, J. S.; Davidson, M. W.; Lippincott-Schwartz, J.; Hess, H. F. Imaging Intracellular Fluorescent Proteins at Nanometer Resolution. *Science* **2006**, *313*, 1642–5.
5. Rust, M. J.; Bates, M.; Zhuang, X. W. Sub-Diffraction-Limit Imaging by Stochastic Optical Reconstruction Microscopy (Storm). *Nat. Methods* **2006**, *3*, 793–795.
6. Heilemann, M.; van de Linde, S.; Schuttpelz, M.; Kasper, R.; Seefeldt, B.; Mukherjee, A.; Tinnefeld, P.; Sauer, M. Subdiffraction-Resolution Fluorescence Imaging with Conventional Fluorescent Probes. *Angew. Chem., Int. Ed.* **2008**, *47*, 6172–6.
7. Schermelleh, L.; Carlton, P. M.; Haase, S.; Shao, L.; Winoto, L.; Kner, P.; Burke, B.; Cardoso, M. C.; Agard, D. A.; Gustafsson, M. G. L.; Leonhardt, H.; Sedat, J. W. Subdiffraction Multicolor Imaging of the Nuclear Periphery with 3D Structured Illumination Microscopy. *Science* **2008**, *320*, 1332–1336.
8. Gustafsson, M. G. L.; Shao, L.; Carlton, P. M.; Wang, C. J. R.; Golubovskaya, I. N.; Cande, W. Z.; Agard, D. A.; Sedat, J. W. Three-Dimensional Resolution Doubling in Wide-Field Fluorescence Microscopy by Structured Illumination. *Biophys. J.* **2008**, *94*, 4957–4970.
9. Gustafsson, M. G. Nonlinear Structured-Illumination Microscopy: Wide-Field Fluorescence Imaging with Theoretically Unlimited Resolution. *Proc. Natl. Acad. Sci. U.S.A.* **2005**, *102*, 13081–6.
10. Heintzmann, R.; Cremer, C. Laterally Modulated Excitation Microscopy: Improvement of Resolution by Using a Diffraction Grating. *Proc. SPIE* **1999**, *3568*, 185–196.
11. Dertinger, T.; Colyer, R.; Iyer, G.; Weiss, S.; Enderlein, J. Fast, Background-Free, 3D Super-Resolution Optical Fluctuation Imaging (SOFI). *Proc. Natl. Acad. Sci. U.S.A.* **2009**, *106*, 22287–92.
12. Michalet, X.; Pinaud, F. F.; Bentolila, L. A.; Tsay, J. M.; Doose, S.; Li, J. J.; Sundaresan, G.; Wu, A. M.; Gambhir, S. S.; Weiss, S. Quantum Dots for Live Cells, *in Vivo* Imaging, and Diagnostics. *Science* **2005**, *307*, 538–544.
13. Rittweger, E.; Han, K. Y.; Irvine, S. E.; Eggeling, C.; Hell, S. W. STED Microscopy Reveals Crystal Colour Centres with Nanometric Resolution. *Nat. Photonics* **2009**, *3*, 144–147.
14. Han, K. Y.; Willig, K. I.; Rittweger, E.; Jelezko, F.; Eggeling, C.; Hell, S. W. Three-Dimensional Stimulated Emission Depletion Microscopy of Nitrogen-Vacancy Centers in Diamond Using Continuous-Wave Light. *Nano Lett.* **2009**, *9*, 3323–3329.
15. Qian, X. M.; Nie, S. M. Single-Molecule and Single-Nanoparticle Sers: From Fundamental Mechanisms to Biomedical Applications. *Chem. Soc. Rev.* **2008**, *37*, 912–920.
16. Zumbusch, A.; Holtom, G. R.; Xie, X. S. Three-Dimensional Vibrational Imaging by Coherent Anti-Stokes Raman Scattering. *Phys. Rev. Lett.* **1999**, *82*, 4142–4145.
17. Freudiger, C. W.; Min, W.; Saar, B. G.; Lu, S.; Holtom, G. R.; He, C. W.; Tsai, J. C.; Kang, J. X.; Xie, X. S. Label-Free Biomedical Imaging with High Sensitivity by Stimulated Raman Scattering Microscopy. *Science* **2008**, *322*, 1857–1861.
18. Stiles, P. L.; Dieringer, J. A.; Shah, N. C.; Van Duyne, R. P. Surface-Enhanced Raman Spectroscopy. *Annu. Rev. Anal. Chem.* **2008**, *1*, 601–626.
19. Wustholz, K. L.; Henry, A. I.; McMahon, J. M.; Freeman, R. G.; Valley, N.; Piotti, M. E.; Natan, M. J.; Schatz, G. C.; Van Duyne, R. P. Structure−Activity Relationships in Gold Nanoparticle Dimers and Trimers for Surface-Enhanced Raman Spectroscopy. *J. Am. Chem. Soc.* **2010**, *132*, 10903–10910.
20. Zavaleta, C. L.; Smith, B. R.; Walton, I.; Doering, W.; Davis, G.; Shojaei, B.; Natan, M. J.; Gambhir, S. S. Multiplexed Imaging of Surface Enhanced Raman Scattering Nanotags in Living Mice Using Noninvasive Raman Spectroscopy. *Proc. Natl. Acad. Sci. U.S.A.* **2009**, *106*, 13511–13516.
21. Sha, M. Y.; Xu, H. X.; Natan, M. J.; Cromer, R. Surface-Enhanced Raman Scattering Tags for Rapid and Homogeneous Detection of Circulating Tumor Cells in the Presence of Human Whole Blood. *J. Am. Chem. Soc.* **2008**, *130*, 17214–17215.
22. Doering, W. E.; Piotti, M. E.; Natan, M. J.; Freeman, R. G. SERS as a Foundation for Nanoscale, Optically Detected Biological Labels. *Adv. Mater.* **2007**, *19*, 3100–3108.
23. Lesterlin, C.; Ball, G.; Schermelleh, L.; Sherratt, D. J. RecA Bundles Mediate Homology Pairing between Distant Sisters during DNA Break Repair. *Nature* **2014**, *506*, 249–253.
24. Svistounov, D.; Warren, A.; McNerney, G. P.; Owen, D. M.; Zencak, D.; Zykova, S. N.; Crane, H.; Huser, T.; Quinn, R. J.; Smedsrod, B.; Le Couteur, D. G.; Cogger, V. C. The Relationship between Fenestrations, Sieve Plates and Rafts in Liver Sinusoidal Endothelial Cells. *PLoS One* **2012**, *7*, e46134.
25. Cogger, V. C.; McNerney, G. P.; Nyunt, T.; DeLeve, L. D.; McCourt, P.; Smedsrod, B.; Le Couteur, D. G.; Huser, T. R. Three-Dimensional Structured Illumination Microscopy of Liver Sinusoidal Endothelial Cell Fenestrations. *J. Struct. Biol.* **2010**, *171*, 382–388.
26. Fiolka, R.; Shao, L.; Rego, E. H.; Davidson, M. W.; Gustafsson, M. G. Time-Lapse Two-Color 3D Imaging of Live Cells with Doubled Resolution Using Structured Illumination. *Proc. Natl. Acad. Sci. U.S.A.* **2012**, *109*, 5311–5315.
27. Shao, L.; Kner, P.; Rego, E. H.; Gustafsson, M. G. L. Super-Resolution 3D Microscopy of Live Whole Cells Using Structured Illumination. *Nat. Methods* **2011**, *8*, 1044–1046.

28. Kner, P.; Chhun, B. B.; Griffis, E. R.; Winoto, L.; Gustafsson, M. G. L. Super-Resolution Video Microscopy of Live Cells by Structured Illumination. *Nat. Methods* **2009**, *6*, 339–342.
29. Schwartzberg, A. M.; Oshiro, T. Y.; Zhang, J. Z.; Huser, T.; Talley, C. E. Improving Nanoprobes Using Surface-Enhanced Raman Scattering from 30 nm Hollow Gold Particles. *Anal. Chem.* **2006**, *78*, 4732–4736.
30. Talley, C. E.; Jusinski, L.; Hollars, C. W.; Lane, S. M.; Huser, T. Intracellular pH Sensors Based on Surface-Enhanced Raman Scattering. *Anal. Chem.* **2004**, *76*, 7064–7068.
31. Michaels, A. M.; Jiang, J.; Brus, L. Ag Nanocrystal Junctions as the Site for Surface-Enhanced Raman Scattering of Single Rhodamine 6G Molecules. *J. Phys. Chem. B* **2000**, *104*, 11965–11971.
32. Talley, C. E.; Jackson, J. B.; Oubre, C.; Grady, N. K.; Hollars, C. W.; Lane, S. M.; Huser, T.; Nordlander, P.; Halas, N. J. Surface-Enhanced Raman Scattering from Individual Au Nanoparticles and Nanoparticle Dimer Substrates. *Nano Lett.* **2005**, *5*, 1569–1574.
33. Aitken, C. E.; Marshall, R. A.; Puglisis, J. D. An Oxygen Scavenging System for Improvement of Dye Stability in Single-Molecule Fluorescence Experiments. *Biophys. J.* **2008**, *94*, 1826–1835.
34. Schaefer, L. H.; Schuster, D.; Schaffer, S. Structured Illumination Microscopy: Artefact Analysis and Reduction Utilizing a Parameter Optimization Approach. *J. Microsc.* **2004**, *216*, 165–174.
35. Blackie, E. J.; Le Ru, E. C.; Etchegoin, P. G. Single-Molecule Surface-Enhanced Raman Spectroscopy of Nonresonant Molecules. *J. Am. Chem. Soc.* **2009**, *131*, 14466–14472.
36. Juan, M. L.; Plain, J.; Bachelot, R.; Royer, P.; Gray, S. K.; Wiederrecht, G. P. Multiscale Model for Photoinduced Molecular Motion in Azo Polymers. *ACS Nano* **2009**, *3*, 1573–1579.
37. Peyser-Capadona, L.; Zheng, J.; Gonzalez, J. I.; Lee, T. H.; Patel, S. A.; Dickson, R. M. Nanoparticle-Free Single Molecule Anti-Stokes Raman Spectroscopy. *Phys. Rev. Lett.* **2005**, *94*, 058301.
38. Zheng, J.; Zhang, C. W.; Dickson, R. M. Highly Fluorescent, Water-Soluble, Size-Tunable Gold Quantum Dots. *Phys. Rev. Lett.* **2004**, *93*, 077402.
39. Choi, S.; Dickson, R. M.; Yu, J. H. Developing Luminescent Silver Nanodots for Biological Applications. *Chem. Soc. Rev.* **2012**, *41*, 1867–1891.
40. Choi, S. M.; Yu, J. H.; Patel, S. A.; Tzeng, Y. L.; Dickson, R. M. Tailoring Silver Nanodots for Intracellular Staining. *Photochem. Photobiol. Sci.* **2011**, *10*, 109–115.
41. Yu, J. H.; Choi, S. M.; Richards, C. I.; Antoku, Y.; Dickson, R. M. Live Cell Surface Labeling with Fluorescent Ag Nanocluster Conjugates. *Photochem. Photobiol.* **2008**, *84*, 1435–1439.
42. Mulvaney, S. P.; Musick, M. D.; Keating, C. D.; Natan, M. J. Glass-Coated, Analyte-Tagged Nanoparticles: A New Tagging System Based on Detection with Surface-Enhanced Raman Scattering. *Langmuir* **2003**, *19*, 4784–4790.